Curvature-Induced Asymmetric Spin-Wave Dispersion

Jorge A. Otálora
Departamento de Física, Universidad Técnica Federico Santa María, Avenida España 1680, Casilla 110-V, Valparaíso, Chile and Departamento de Física, CEDENNA, Universidad Santiago de Chile, USACH, 9170124 Santiago, Chile

Ming Yan
Department of Physics, Shanghai University, 99 Shangda Road, BaoShan District, Shanghai 200444, China

Helmut Schultheiss
Helmholtz-Zentrum Dresden—Rossendorf, Institute of Ion Beam Physics and Materials Research, Bautzner Landstraße 400, 01328 Dresden, Germany and Technische Universität Dresden, D-01062 Dresden, Germany

Riccardo Hertel
Karlsuhe Institute of Technology, Physikalisches Institut, Wolfgang-Gaede-Str. 1, D-76131 Karlsruhe, Germany and Institut de Physique et Chimie des Matériaux de Strasbourg, UMR 7504, CNRS, and Université de Strasbourg, 23 rue du Loess, F-67300 Strasbourg, France

Attila Kákay*
Helmholtz-Zentrum Dresden—Rossendorf, Institute of Ion Beam Physics and Materials Research, Bautzner Landstraße 400, 01328 Dresden, Germany

(Received 5 May 2016; published 23 November 2016)

In magnonics, spin waves are conceived of as electron-charge-free information carriers. Their wave behavior has established them as the key elements to achieve low power consumption, fast operative rates, and good packaging in magnon-based computational technologies. Hence, knowing alternative ways that reveal certain properties of their undulatory motion is an important task. Here, we show using micromagnetic simulations and analytical calculations that spin-wave propagation in ferromagnetic nanotubes is fundamentally different than in thin films. The dispersion relation is asymmetric regarding the sign of the wave vector. It is a purely curvature-induced effect and its fundamental origin is identified to be the classical dipole-dipole interaction. The analytical expression of the dispersion relation has the same mathematical form as in thin films with the Dzyalonshiinsky-Moriya interaction. Therefore, this curvature-induced effect can be seen as a "dipole-induced Dzyalonshiinsky-Moriya-like" effect.

DOI: 10.1103/PhysRevLett.117.227203

Using the electron's spin degree of freedom for data processing instead of its charge is one great challenge. The first success story can nowadays be seen in spintronic devices employing various magnetoresistance effects in magnetic sensors and storage applications. About ten years ago a new research field called magnonics emerged driven by the idea to use magnons as carrier of spin information [1–8]. Magnons, also called spin waves (SWs), are the dynamic eigenoscillations of the spin system in ferromagnets with frequencies in the gigahertz to terahertz range and with nanometer wavelengths. Novel materials allow for the coherent propagation of SWs over mesoscopic distances without any charge transport involved, paving the way for green data processing. Many concepts have been proposed theoretically and experimentally, leading to prototype building blocks of spin-wave-based logic [8–13]. The experimental discovery of novel phenomena such as the spin Hall effect, the Dzyaloshinski-Moria interaction [14,15] (DMI), the spin Seebeck effect, and others proved powerful mechanisms to excite, manipulate, and detect SWs in thin magnetic films on the nanometer scale via coupling of the magnons to charge and heat transport. One particular feature of SWs in thin films is intriguing: A certain set of SWs known as Damon-Eshbach (DE) [16] modes show a nonreciprocity regarding the inversion of the wave vector caused by dipolar interaction. When the propagation direction is reversed, these magnons switch from the top to the bottom surface of the thin film. Recently it was discovered that an asymmetric exchange interaction (DMI) in ultrathin ferromagnetic films can also cause an asymmetric SW dispersion [17], i.e., one can switch from positive to negative dispersion upon reversal of the wave vector. In this Letter we show that one can obtain a similar asymmetric SW dispersion that is purely caused by dipolar interaction when going from thin films to three-dimensional structures with curved surfaces, in particular magnetic nanotubes (MNTs). Such novel structures can nowadays be very well produced [18,19], motivated by the broad range of applications for magnetoresistive devices, optical metamaterials, cell-DNA separators, and drug

delivery vectors [20,21]. The high stability of their equilibrium state [22,23] against external perturbations and their robust domain walls propagating with velocities faster than the SW phase velocity [24] promote MNTs as appealing candidates for racetrack memory devices [25,26] and information processing [24,27].

In this Letter, we report the numerical simulation and full analytical description of curvature-induced asymmetric SW dispersion in nanotubes, which has the same mathematical form [28–31] as the DMI but identifies the dipole-dipole interaction as the origin of the asymmetry. We demonstrate that the degree of asymmetry can be tuned with the tube geometry but also with small electric currents flowing through the nanotube. Besides the tunability, contrary to thin films with the DMI, the asymmetry is present and is significant even in the absence of external magnetic fields.

Finite element micromagnetic simulations [32,33] were performed to study the propagation of SWs in MNTs. The numerical research is focused on a tube defined by an outer radius $R = 30$ nm, a wall thickness $d = 10$ nm, and a length $L = 4\ \mu$m. The MNT is assumed to be made of permalloy and the following material parameters are used: saturation magnetization $\mu_0 M_s = 1$ T, exchange stiffness constant $A = 1.3 \times 10^{-11}$ J/m, negligible magnetocrystalline anisotropy ($K_u = 0$), and low Gilbert damping $\alpha_G = 0.01$. Details of the simulations are presented in the Sec. S1 of the Supplemental Material [34].

The propagation and dispersion of SWs in MNTs are simulated for an equilibrium state in which the magnetization rotates around the circumference of the tube, thus forming a perfect flux closure configuration [35,36]. This state in the following is referenced as a vortex (V) configuration. It is not a ground state for the given geometry and an external field is required to stabilize it. A circular Oersted field $H_0 \geq H_{\text{crit}}$ induced by a current flowing through the MNT or its core can serve this function. The critical field for the nanotube with the described geometry is $\mu_0 H_{\text{crit}} = 53$ mT [37].

A schematic of the considered system is shown in Fig. 1(a) with the tube in the V state together with the polar coordinate system used throughout the Letter, where ρ, φ, and z are the radial, azimuthal, and long axis coordinates. The SWs are excited with a homogeneous rf field applied in the radial direction at the middle of the tube in a 100 nm wide region, as indicated with the orange ring in Fig. 1(a). The SWs propagate from the middle of the nanotube toward its ends with wave vector k_z. The circulation direction of the magnetization $\hat{\varphi}$ together with the propagation direction $\hat{z}$ defines a chirality or handedness. The direction of propagation is shown in all figures such that SWs propagating to the right (left) with $k_R \equiv +|k_z|$ ($k_L \equiv -|k_z|$) define the right- (left-)handed (RH and LH) chirality. Since the propagation direction is perpendicular to the magnetization, similar to thin films, this excitation geometry is addressed as the Damon-Eshbach geometry.

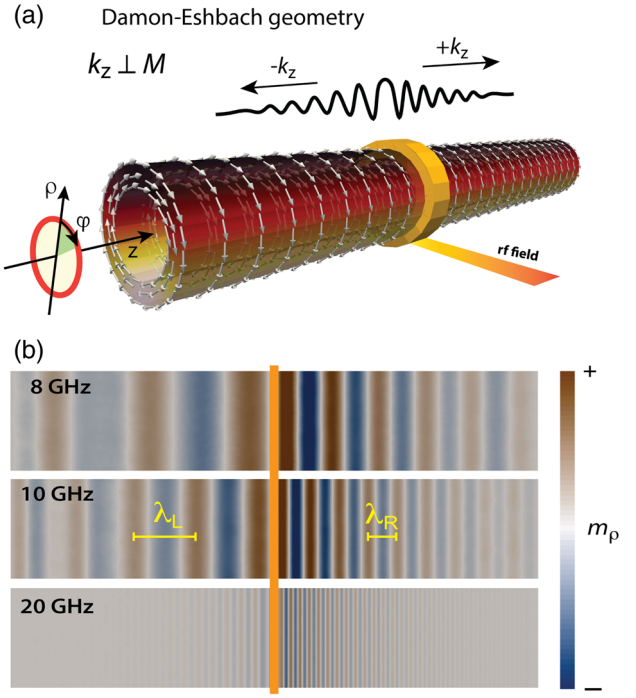

FIG. 1. (a) Schematic illustration of a nanotube in a vortex state and the cylindrical coordinate system. SWs are excited in the middle with a radial rf field, as illustrated by the orange ring. The SWs travel toward the ends of the nanotube with a wave vector k_z perpendicular to the magnetization. $+k_z$ and $-k_z$ indicate the right and left propagation directions, respectively. (b) A snapshot in time of the SW profiles (radial component of the magnetization color coded) for the three different excitation frequencies 8, 10 and 20 GHz for a circular field of 80 mT. The orange bar indicates the position and width of the rf field. $\lambda_L(\lambda_R)$ denotes the wavelength of the waves traveling to the left (right).

The SW excitation and propagation were simulated for several values of the circular field. For all field values, the continuous rf field exciting the SWs is applied until the steady state is reached. Figure 1(b) shows a snapshot in time of the SW profiles for the three different excitation frequencies 8, 10, and 20 GHz for a circular field of 80 mT, well above the critical field. The color scheme represents the radial component of the magnetization in an unrolled view. The rf-field position is illustrated with an orange bar. λ_L and λ_R denote the wavelength of the SWs on the left and right of the excitation region, respectively. Remarkably, the wavelength of the SWs propagating to the left differs from those propagating to the right. This difference in wavelength decreases with increasing excitation frequencies, but never vanishes, according to the micromagnetic simulations for the considered range of frequencies.

Figure 2 shows the SW dispersion obtained from the micromagnetic simulations for two different values of the circular field, 80 mT and 1 T. The dispersion is asymmetric regarding the propagation direction and moreover, the minimum of the dispersion depends on the circular field as seen by comparing Figs. 2(a) and 2(b). Despite the

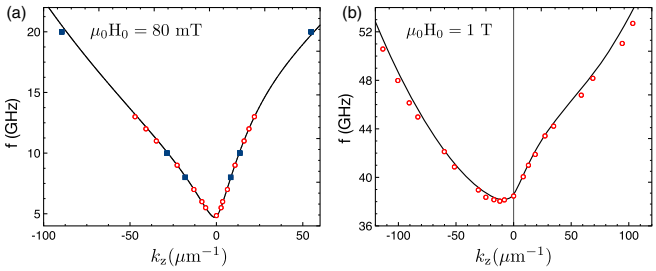

FIG. 2. SW dispersion relation obtained by micromagnetic simulations (red and blue dots) and analytical calculations (solid line) for circular fields of 80 mT (a) and 1 T (b). The blue squares mark the frequencies for which the SW profile is shown in Fig. 1(b). A nearly perfect agreement between the results of the micromagnetic simulations and the analytical calculations is found.

geometrical similarity, our simulations show that the DE modes in nanotubes behave differently than their thin-film counterparts. Simulations suggest that for $k_z = k_L$ there is a range of wave vectors wherein the group velocity is negative, specific to the backward volume modes in thin films. A similar effect has been recently reported for thin films with the Dzyalonshinskii-Moriya interaction [17,28–31].

For a deeper understanding of the origin of the asymmetry observed in the simulations, an analytical formula for the SW dispersion of nanotubes is presented. The analytical description is given under the framework of micromagnetic continuum theory. The dispersion relation is calculated by (i) linearizing the Landau-Lifshitz-Gilbert equation, and (ii) solving the linear equation in terms of individual magnons with wave vector k_z along the nanotube axis $\hat{z}$, with an integer wave number n characteristic of the azimuthal symmetry along $\hat{\varphi}$, and with eigenfrequency $\omega_n(k_z)$. An extensive analytical derivation presented in Ref. [38] (guidelines can also be found in the Sec. S2 of the Supplemental Material [34]) leads to the following dispersion relation for the coherently distributed SWs [$n = 0$; SWs with planar wave mode profiles as shown in Fig. 1(b)] along the $\hat{\varphi}$ axis:

$$\frac{\omega_0(k_z)}{\gamma_0 \mu_0 M_s} = \mathcal{K}_0(k_z) + \sqrt{\mathcal{A}_0(k_z)\mathcal{B}_0(k_z)}, \tag{1}$$

where the quantities $\mathcal{A}_0$ and $\mathcal{B}_0$ are defined as

$$\begin{aligned} \mathcal{A}_0(k_z) &= l_{\mathrm{ex}}^2\left(k_z^2 - \frac{1}{b^2}\right) + h_0 + \mathcal{L}_0(k_z), \\ \mathcal{B}_0(k_z) &= l_{\mathrm{ex}}^2 k_z^2 + h_0 + \mathcal{J}_0(k_z) \end{aligned} \tag{2}$$

with the functions $\mathcal{J}_0$, $\mathcal{K}_0$, and $\mathcal{L}_0$ given by

$$\begin{aligned} \mathcal{J}_0(k_z) &= \frac{\pi}{S}\int_0^\infty dk \frac{k^3}{2(k^2+k_z^2)}[\Gamma_0(k)]^2, \\ \mathcal{K}_0(k_z) &= \frac{\pi}{S}\int_0^\infty dk \frac{k^2 k_z}{k^2+k_z^2}\Gamma_0(k)\Lambda_0(k), \\ \mathcal{L}_0(k_z) &= \frac{\pi}{S}\int_0^\infty dk \frac{2kk_z^2}{k^2+k_z^2}[\Lambda_0(k)]^2 \end{aligned} \tag{3}$$

with $\Lambda_0(k) = \int_r^R d\rho\rho J_0(k\rho)$, $\Gamma_0(k) = -2\Lambda_1(k)$, $J_0(x)$ is the first kind of Bessel function of zero order, $b^{-2} = 2\pi \ln(R/r)/S$, and $S = \pi(R^2 - r^2)$ the nanotube cross section, with R and r being the outer and inner radius, respectively. $l_{\mathrm{ex}} = \sqrt{A/K_d}$ is the exchange length, A is the exchange stiffness constant, $K_d = (1/2)\mu_0 M_s^2$ is the shape anisotropy constant, and h_0 is the circular field normalized to the saturation magnetization M_s.

Figures 2(a) and 2(b) show the dispersion calculated with Eq. (1). The solid line representing the analytical calculations is in perfect agreement with the results of the simulations.

Using Eq. (1), the SW dispersion is calculated for tubes with different diameters and a varying circular field. Two cases are summarized for tubes with a 10 nm film thickness and an outer radius of 30 and 150 nm in Figs. 3(a) and 3(b), respectively. As shown, the minima of the dispersion is shifted towards larger k_z values with increasing circular field, allowing for the manipulation of the asymmetry and the wave vector ranges for which the SWs have a negative group velocity. However, the asymmetry is decreased with increasing outer diameter since the curvature is reduced and completely vanishes for infinite diameters at the thin film limit. It is noteworthy that Eq. (1) allows for a systematic study of the eigenoscillations and its features $[k_z, \omega_0(k_z)]$ as a function of nanotube size, material parameters, and applied circular and/or axial fields without the need for expensive micromagnetic simulations.

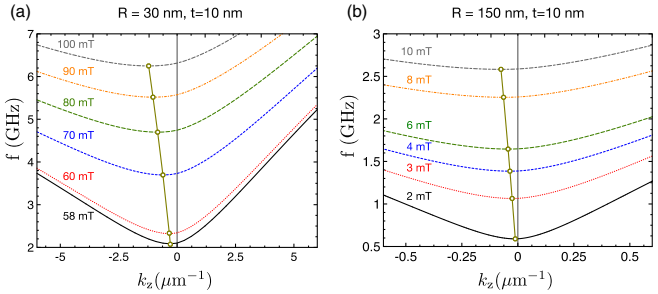

FIG. 3. The dispersion of SWs is summarized for several circular fields as a function of wave number for nanotubes with (a) 30 nm and (b) 150 nm outer radius and a 10 nm film thickness. The minima of the dispersion are shifted towards larger k_z values with increasing circular field for both diameters. The open dots represent the minima for each circular field and the solid line connecting them is a guide to the eye only.

The asymmetric SW dispersion reported in this Letter cannot be explained within the classical frame of the DE dispersion known for thin films. The DE modes in nanotubes with negative k_z behave as volume-charge-free backward volume modes in thin films. Such an effect, however, is already known for thin films [17] with antisymmetric exchange (DMI) due to spin-orbit coupling. In fact the DMI favors a canting of the spins with a given chirality and therefore introduces a local symmetry break that can lead to an asymmetric dispersion relation [28–31]. Nevertheless, for nanotubes the source of the asymmetric dispersion resides only in the dipole-dipole interaction, which is discussed in the following.

Note that Eq. (1) has the same mathematical form as in thin films with an interfacial DMI or in crystals with a special symmetry (C_{nv}) and a bulk DMI [see Eqs. (6)–(9) in Ref. [30] and Table 1 in Ref. [28]]. $\mathcal{K}_0(k_z)$ plays the same role in nanotubes as the well-known asymmetrical terms in thin films (crystals) with an interfacial (bulk) DMI (i.e., the term $(2\gamma_0/M_s)Dk$ in the dispersion of thin films with an interfacial DMI [30], where D is the DMI constant) but with the difference that $\mathcal{K}_0(k_z)$ originates from the dynamic volume charges created by the SWs as a result of the tubular curvature. From Eq. (3) it is easy to see that $\mathcal{K}_0(k_z)$ is an odd function [i.e., $\mathcal{K}_0(k_z) = -\mathcal{K}_0(-k_z)$], therefore being the asymmetrical term in the dispersion relation.

The term $\mathcal{K}_0(k_z)$, which can only be calculated by numerical integration of the corresponding Bessel functions, comprises the dynamic dipolar energy arising from the surface as well as from the volume charges [39] $\rho_v \equiv -(M_s/4\pi)\vec{\nabla}\cdot\vec{M}$. The negative dispersion or negative group velocity, however, should be related to small or close to zero volume charges. With the magnetization in the vortex state for a SW with wave vector k_z, wave number $n = 0$, and eigenfrequency ω, the volume charges averaged over the nanotube radius are $\langle\rho_V\rangle = \langle\rho_V\rangle_0 e^{i(k_z z-\omega t+\xi)}$ with

$$\langle\rho_V\rangle_0 = -\frac{M_s^2}{4\pi}\left(\frac{1}{\bar{\rho}} + k_z\sqrt{\frac{\mathcal{B}_0(k_z)}{\mathcal{A}_0(k_z)}}\right)\left(1+\frac{\mathcal{B}_0(k_z)}{\mathcal{A}_0(k_z)}\right)^{-\frac{1}{2}}, \quad (4)$$

where $\mathcal{A}_0(k_z)$ and $\mathcal{B}_0(k_z)$ are defined in Eq. (2); ξ is the phase constant of the radial and axial SW components. It can be seen that the amplitude is proportional to two terms. The first term $1/\bar{\rho}$ is the inverse of the nanotube average radius, which is proportional to the mean nanotube curvature [40]. The second term $k_z\sqrt{[\mathcal{B}_0(k_z)/\mathcal{A}_0(k_z)]}$ depends on the propagation vector k_z. Hence, the sum of the two terms depends on the sign of k_z. Therefore, for opposite propagation directions the dynamic volume charges are different.

In Fig. 4(a) the volume charge amplitude as a function of wave vector is shown for nanotubes with three different radii. As expected from the previous considerations, it has

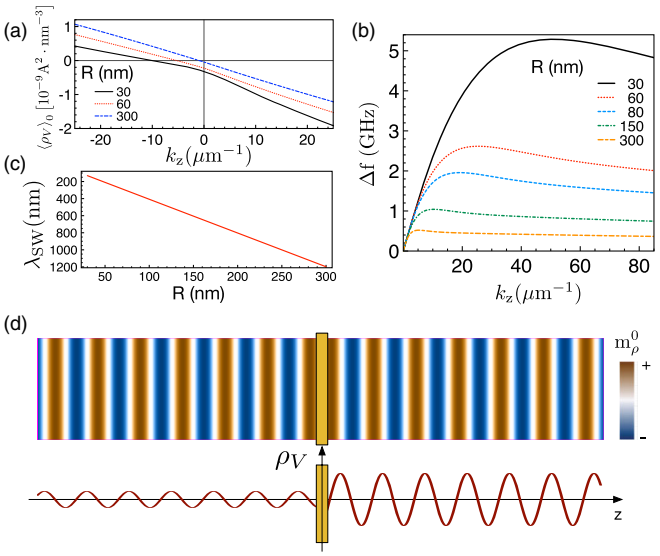

FIG. 4. (a) The volume charge amplitude as a function of wave vector. (b) SW asymmetry as a function of wave vector k_z for nanotubes with varying radius. (c) The wavelength λ_{SW} of the excited SWs for which the maximum asymmetry is reached versus the nanotube radius. (d) SW profile for waves with equal wavelength but opposite travel direction and the corresponding volume charges. The color scheme encodes the radial component of the dynamic magnetization. The dark yellow rectangles mark the excitation region.

an asymmetric dependence on k_z. Moreover, zero volume charges are obtained for k_z values different from zero. Around these k_z values the reduction in energy from the surface charges is larger than the energy increase from the volume charges; thus, the total energy decreases, leading to a negative dispersion.

In Fig. 4(d) the SW profile as well as the divergence calculated with our TetraMag [32,33] code is shown for a case when the SWs propagating towards opposite ends have the same wavelength. Clearly, the resulting dynamic volume charges and thus the dipolar energies differ for the two sides. In experiments (or simulations) the excitation is done with a well defined frequency; therefore, the SW's should possess the same energy for the opposite travel directions. In nanotubes this can only be reached if the wavelengths differ such that the dynamic dipolar energy resulting from the surface and volume charges is the same for the two propagation directions. As a consequence SWs propagating in opposite directions have different wavelengths and show an asymmetric dispersion. It is worth mentioning that the dipole-dipole interaction was reported to be also responsible for the asymmetric domain wall propagation in nanotubes [41].

The SW asymmetry defined as the frequency difference of the SWs traveling in opposite directions but with the same wave vector is also proportional to the asymmetrical term and can be calculated analytically using Eq. (1). It reads

$$\Delta f = \frac{\gamma M_s}{2\pi}|\omega_0(k_z) - \omega_0(-k_z)| = \frac{\gamma M_s}{\pi}|\mathcal{K}_0(k_z)|. \quad (5)$$

The SW asymmetry can be estimated from Eq. (3) by looking at the dependence of $\mathcal{K}_0(k_z)$ on the value of k_z. Equation (5) as a function of wave vector is plotted for nanotubes with different radii in Fig. 4(b). It can be seen that the maximum frequency difference decreases with increasing tube radius. For tubes with a small diameter this value is in the range of several gigahertz; however, for tubes 500–600 nm in diameter—which are accessible experimentally due to the recent progress in material science [18]—the frequency difference is still in the range of several hundred megahertz. The SW wavelength for which the maximum asymmetry is reached is shown in Fig. 4(c) as a function of the nanotube outer radius. It is in perfect agreement with our simple predictions based on the volume charges; namely, the asymmetry (smallest contribution of the volume charges to the total energy) is largest for wavelengths comparable to the nanotube diameter.

In a final step two limiting cases of the dispersion are presented: (1) $k_z = 0$, and (2) $k_z \gg 1/R$. For $k_z = 0$ the dispersion has the following form $\omega_{\mathrm{FMR}} = \gamma_0\mu_0\sqrt{(H_0 - H_u)(H_0 + M_s)}$, which resembles the Kittel formula for the ferromagnetic resonance (FMR) of a thin film with the in-plane magnetization parallel to the applied field, and both oriented perpendicularly to the in-plane easy axis of the shape anisotropy field H_u. For a large radius, $H_u \ll H_0$; therefore, the well-known FMR formula [42] $\omega_{\mathrm{FMR}} \approx \gamma_0\mu_0\sqrt{H_0(H_0 + M_s)}$ for thin films with a homogeneous in-plane magnetization parallel to the applied magnetic field H_0 is obtained.

For a very small wavelength, $k_z \gg 1/R$, the dispersion can be written as

$$\omega_0(k_z) \approx \gamma_0\mu_0\sqrt{(M_s l_{\mathrm{ex}}^2 k_z^2 - H_u + H_0 + M_s)(M_s l_{\mathrm{ex}}^2 k_z^2 + H_0)}, \quad (6)$$

which is identical to the exchange-dominated dispersion relation of a planar thin film in the Damon-Esbach configuration with the in-plane magnetization oriented perpendicularly to the in-plane easy axis [16,43] (The derivation of the asymptotic analytical expressions is summarized in Ref. [38]).

In summary, we have shown using micromagnetic simulations as well as analytical calculations that SW propagation in nanotubes is fundamentally different than in thin films. The observed asymmetric dispersion is a purely curvature-induced effect [44–46] and can be tuned with small electrical currents. We have shown that the SW asymmetry is in the megahertz to gigahertz range in frequency and depends on the nanotube radius. The analytical expression of the dispersion has the same mathematical form as in thin films with the Dzyalonshiinsky-Moriya interaction. The fundamental origin of the asymmetric dispersion is the classical dipole-dipole interaction; therefore. it can be seen as a "dipole-induced DMI-like effect." We hope that the results presented here will encourage the experimental verification of this curvature-induced effect.

Financial support by the Centers of Excellence with BASAL/CONICYT financing, CEDENNA No. FB0807, and Project FONDECYT Regular No. 1161403 is gratefully acknowledged. A. K. would like to acknowledge helpful discussions with J. Lindner and J. Fassbender. M. Y. is supported by the National Natural Science Foundation of China (Grant No. 11374203) and the Shanghai Key Laboratory of High Temperature Superconductors (Grant No. 14DZ2260700). H. S. acknowledges financial support from the Deutsche Forschungsgemeinschaft within programme SCHU 2922/1-1. Also, the authors are very grateful to R. Gallardo for fruitful discussions.

*a.kakay@hzdr.de

[1] V. Kruglyak and R. Hicken, J. Magn. Magn. Mater. **306**, 191 (2006).
[2] S. Neusser and D. Grundler, Adv. Mater. **21**, 2927 (2009).
[3] A. Khitun, M. Bao, and K. L. Wang, J. Phys. D **43**, 264005 (2010).
[4] V. V. Kruglyak, S. O. Demokritov, and D. Grundler, J. Phys. D **43**, 264001 (2010).
[5] D. Grundler, Nat. Phys. **11**, 438 (2015).
[6] B. Lenk, H. Ulrichs, F. Garbs, and M. Münzenberg, Phys. Rep. **507**, 107 (2011).
[7] A. V. Chumak, V. I. Vasyuchka, A. A. Serga, and B. Hillebrands, Nat. Phys. **11**, 453 (2015).
[8] R. Hertel, W. Wulfhekel, and J. Kirschner, Phys. Rev. Lett. **93**, 257202 (2004).
[9] A. V. Chumak, A. A. Serga, and B. Hillebrands, Nat. Commun. **5**, 4700 (2014).
[10] K. Vogt, F. Y. Fradin, J. E. Pearson, T. Sebastian, S. D. Bader, B. Hillebrands, A. Hoffmann, and H. Schultheiss, Nat. Commun. **5** (2014).
[11] K. Wagner, A. Kákay, K. Schultheiss, A. Henschke, T. Sebastian, and H. Schultheiss, Nat. Nanotechnol. **11**, 432 (2016).
[12] S. Urazhdin, V. E. Demidov, H. Ulrichs, T. Kendziorczyk, T. Kuhn, J. Leuthold, G. Wilde, and S. O. Demokritov, Nat. Nanotechnol. **9**, 509 (2014).
[13] A. Haldar, D. Kumar, and A. O. Adeyeye, Nat. Nanotechnol. **11**, 437 (2016).
[14] I. Dzyaloshinsky, J. Phys. Chem. Solids **4**, 241 (1958).
[15] T. Moriya, Phys. Rev. **120**, 91 (1960).
[16] R. Damon and J. Eshbach, J. Phys. Chem. Solids **19**, 308 (1961).
[17] K. Zakeri, Y. Zhang, J. Prokop, T.-H. Chuang, N. Sakr, W. X. Tang, and J. Kirschner, Phys. Rev. Lett. **104**, 137203 (2010).

[18] K. Nielsch, F. Castaño, S. Matthias, W. Lee, and C. Ross, Adv. Eng. Mater. **7**, 217 (2005).
[19] M. Vázquez, *Magnetic Nano- and Microwires*, 1st ed. (Elsevier, New York, 2016).
[20] D. F. Emerich and C. G. Thanos, Expert Opin. Biol. Ther. **3**, 655 (2003).
[21] S. J. Son, J. Reichel, B. He, M. Schuchman, and S. B. Lee, J. Am. Chem. Soc. **127**, 7316 (2005).
[22] R. Streubel, L. Han, F. Kronast, A. A. Ünal, O. G. Schmidt, and D. Makarov, Nano Lett. **14**, 3981 (2014).
[23] A. Buchter, R. Wölbing, M. Wyss, O. F. Kieler, T. Weimann, J. Kohlmann, A. B. Zorin, D. Rüffer, F. Matteini, G. Tütüncüoglu, F. Heimbach, A. Kleibert, A. Fontcuberta i Morral, D. Grundler, R. Kleiner, D. Koelle, and M. Poggio, Phys. Rev. B **92**, 214432 (2015).
[24] M. Yan, C. Andreas, A. Kákay, F. García-Sánchez, and R. Hertel, Appl. Phys. Lett. **99**, 122505 (2011).
[25] S. S. P. Parkin, M. Hayashi, and L. Thomas, Science **320**, 190 (2008).
[26] M. Hayashi, L. Thomas, R. Moriya, C. Rettner, and S. S. P. Parkin, Science **320**, 209 (2008).
[27] J. A. Otálora, J. A. López-López, P. Vargas, and P. Landeros, Appl. Phys. Lett. **100**, 072407 (2012).
[28] D. Cortés-Ortuño and P. Landeros, J. Phys. Condens. Matter **25**, 156001 (2013).
[29] F. Ma and Y. Zhou, RSC Adv. **4**, 46454 (2014).
[30] K. Di, V. L. Zhang, H. S. Lim, S. C. Ng, M. H. Kuok, J. Yu, J. Yoon, X. Qiu, and H. Yang, Phys. Rev. Lett. **114**, 047201 (2015).
[31] Y. Iguchi, S. Uemura, K. Ueno, and Y. Onose, Phys. Rev. B **92**, 184419 (2015).
[32] R. Hertel, in *Handbook of Magnetism and Advanced Magnetic Materials* (John Wiley & Sons, New York, 2007), pp. 1003–1020.
[33] A. Kákay, E. Westphal, and R. Hertel, IEEE Trans. Magn. **46**, 2303 (2010).
[34] See Supplemental Material at http://link.aps.org/supplemental/10.1103/PhysRevLett.117.227203, for the details of the micromagnetic simulations and for the guidelines of the analytical derivation of the dispersion relation.
[35] P. Landeros, S. Allende, J. Escrig, E. Salcedo, D. Altbir, and E. Vogel, Appl. Phys. Lett. **90**, 102501 (2007).
[36] P. Landeros, O. J. Suarez, A. Cuchillo, and P. Vargas, Phys. Rev. B **79**, 024404 (2009).
[37] J. A.Otálora, D. Cortés-Ortuño, D. Görlitz, K. Nielsch, and P. Landeros, J. Appl. Phys. **117**, 173914 (2015).
[38] J. A. Otálora, M. Yan, H. Schultheiss, R. Hertel, and A. Kákay (to be published).
[39] W. F. Brown, *Micromagnetics* (Interscience Publishers, New York, 1963).
[40] M. Burger, *S.S. Chern: A Great Geometer of the Twentieth Century, expanded edition* (International Press, Somerville, 2012), p. 184.
[41] M. Yan, C. Andreas, A. Kákay, F. García-Sánchez, and R. Hertel, Appl. Phys. Lett. **100**, 252401 (2012).
[42] C. Kittel, *Introduction to Solid State Physics*, 6th ed. (John Wiley & Sons, Inc., New York, 1986).
[43] B. Kalinikos and A. Slavin, J. Phys. C **19**, 7013 (1986).
[44] B. M. Tanygin, J. Magn. Magn. Mater. **323**, 616 (2011).
[45] R. Hertel, SPIN **3**, 1340009 (2013).
[46] O. V. Pylypovskyi, D. D. Sheka, V. P. Kravchuk, K. V. Yershov, D. Makarov, and Y. Gaididei, Sci. Rep. **6**, 23316 (2016).